Amyloid fibrils from the N-terminal prion protein fragment are infectious

Jin-Kyu Choi[a], Ignazio Cali[b], Krystyna Surewicz[a], Qingzhong Kong[b], Pierluigi Gambetti[b], and Witold K. Surewicz[a,1]

[a]Department of Physiology and Biophysics, Case Western Reserve University, Cleveland, OH 44106; and [b]Department of Pathology, Case Western Reserve University, Cleveland, OH 44106

Edited by Stanley B. Prusiner, University of California, San Francisco, CA, and approved October 14, 2016 (received for review June 30, 2016)

Recombinant C-terminally truncated prion protein PrP23-144 (which corresponds to the Y145Stop PrP variant associated with a Gerstmann–Sträussler–Scheinker-like prion disease) spontaneously forms amyloid fibrils with a parallel in-register β-sheet architecture and β-sheet core mapping to residues ∼112–139. Here we report that mice (both *tga20* and wild type) inoculated with a murine (moPrP23-144) version of these fibrils develop clinical prion disease with a 100% attack rate. Remarkably, even though fibrils in the inoculum lack the entire C-terminal domain of PrP, brains of clinically sick mice accumulate longer proteinase K-resistant (PrP^{res}) fragments of ∼17–32 kDa, similar to those observed in classical scrapie strains. Shorter, Gerstmann–Sträussler–Scheinker-like PrP^{res} fragments are also present. The evidence that moPrP23-144 amyloid fibrils generated in the absence of any cofactors are bona fide prions provides a strong support for the protein-only hypothesis of prion diseases in its pure form, arguing against the notion that nonproteinaceous cofactors are obligatory structural components of all infectious prions. Furthermore, our finding that a relatively short β-sheet core of PrP23-144 fibrils (residues ∼112–139) with a parallel in-register organization of β-strands is capable of seeding the conversion of full-length prion protein to the infectious form has important implications for the ongoing debate regarding structural aspects of prion protein conversion and molecular architecture of mammalian prions.

prion disease | prions | amyloid | infectivity

Transmissible spongiform encephalopathies (TSEs), also known as prion diseases, are a diverse group of neurodegenerative disorders that include Creutzfeldt–Jakob disease (CJD) and Gerstmann–Sträussler–Scheinker (GSS) disease in humans, bovine spongiform encephalopathy in cattle, scrapie in sheep, and chronic wasting disease in cervids (1–3). These disorders may arise spontaneously via inheritance or by way of infection. Conformational conversion of the normally monomeric and α-helical cellular prion protein, PrP^{C}, to a misfolded aggregated form, PrP^{Sc}, underlies the pathogenic mechanisms of all forms of TSE diseases (1–3). The "protein-only" hypothesis asserts that PrP^{Sc} itself is the main, if not sole, component of the infectious prion pathogen (1). Even though this model is supported by large body of experimental data, there is an ongoing dispute regarding the involvement of specific nonproteinaceous cofactors in prion infectivity (4–6). Furthermore, little is known about the mechanism of prion protein conversion and the structure of the infectious prion pathogen.

Apart from the landmark studies with PrP-knockout mice (7), arguably the strongest support for the proteinaceous nature of the TSE pathogen has been provided by experiments using protein misfolding cyclic amplification (PMCA) technology in which PrP^{Sc} is replicated by a procedure involving intermittent cycles of sonication and incubation (8). Using this approach, highly infectious prions were generated from partially purified brain-derived PrP^{C} (4) and, more recently, bacterially expressed highly purified recombinant PrP (rPrP) (5, 6). However, creation of infectious material in these studies required additional cofactors such as polyanions and/or specific phospholipids. Prions were also generated in a seeded PMCA reaction from bacterially expressed hamster rPrP in the absence of any cofactors other than an acidic detergent (SDS), but the infectivity level of the latter material appeared low as indicated by an incomplete attack rate (9).

Using a different approach, a number of studies have tested the infectivity of amyloid fibrils generated from bacterially expressed rPrP or its C-terminal domain (10–17). Some of these synthetic preparations were reported to cause clinical symptoms in transgenic mice overexpressing PrP^{C} (10–12) or coexpressing relatively low levels of wild-type and GPI-anchorless PrP^{C} (16). However, no clinical disease has yet been reported upon primary passage of rPrP amyloid fibrils in wild-type rodents.

Most TSE diseases, including CJD, are associated with the presence in brains of large proteinase K (PK)-resistant prion protein (PrP^{res}) fragments that are ∼19–21 kDa in size (in an unglycosylated form) and typically extend from residues ∼80–90 up to the C terminus (1, 3). By contrast, GSS diseases are typically characterized by amyloid deposits containing relatively short PrP internal fragments (18–20). The most common of these is 6–8 kDa in size; depending on the disease phenotype, this fragment starts at residue 78–88 and ends at residue 144–153. One of GSS-like subtypes is associated with the tyrosine to stop codon mutation in *PRNP* at position 145, resulting in a C-terminally truncated prion protein fragment corresponding to residues 23–144 (PrP23-144) (21, 22). Previously, we showed that bacterially expressed recombinant PrP23-144 from different species readily forms amyloid fibrils under physiological buffer conditions (23), and studies in vitro with this truncated PrP variant revealed mechanistic principles of the conformational basis of species- and strain-dependent seeding specificity of prion protein amyloids (24, 25).

Here, we demonstrate that inoculation of both transgenic (*tga20*) and wild-type mice with amyloid fibrils generated from highly purified recombinant mouse PrP23-144 (moPrP23-144; numbering

Significance

Prion diseases are a group of transmissible neurodegenerative disorders. The protein-only hypothesis asserts that transmission of these diseases does not require nucleic acids and that a misfolded, aggregated form of the prion protein represents a self-perpetuating infectious agent. Even though this model is supported by a large body of experimental data, there is a dispute regarding the role of specific cofactors in prion infectivity as well as the structural basis of prion formation. In this work, we show that structurally well-characterized amyloid fibrils generated from bacterially expressed prion protein fragment 23-144 cause prion disease in transgenic and wild-type mice, demonstrating that cofactors are not obligatory for prion formation and providing insight into the structural basis of prion propagation.

Author contributions: W.K.S. designed research; J.-K.C., I.C., K.S., Q.K., and P.G. performed research; J.-K.C., I.C., P.G., and W.K.S. analyzed data; and J.-K.C., I.C., P.G., and W.K.S. wrote the paper.

The authors declare no conflict of interest.

This article is a PNAS Direct Submission.

[1]To whom correspondence should be addressed. Email: witold.surewicz@case.edu.

This article contains supporting information online at www.pnas.org/lookup/suppl/doi:10.1073/pnas.1610716113/-/DCSupplemental.

according to human PrP sequence) results in clinical prion disease with a 100% attack rate. Remarkably, even though fibrils in the inoculum lack the entire C-terminal domain of PrP, brains of clinically sick mice are characterized by the presence of both short (GSS-like) and long (scrapie-like) PrP^{res} fragments. In addition to demonstrating that cofactor-free, structurally well-characterized amyloid fibrils generated from the N-terminal PrP fragment are bona fide prions, this study provides potentially important clues regarding the mechanism of prion protein conversion to the infectious form.

Results

moPrP23-144 Amyloid Fibrils Can Seed Conversion of Full-Length PrP^{C} to a PK-Resistant Form in Vitro. Detailed characterization of moPrP23-144 fibrillation kinetics and fibril morphology has been described previously (24, 25). Treatment of moPrP23-144 fibrils with PK reveals the presence of ~7-kDa and 5-kDa PK-resistant fragments that, according to mass spectrometric analysis, map to PrP residues 74–144 and 92/98–144, respectively (Fig. S1).

Previous studies have shown that the procedure of serial PMCA provides an efficient tool for the replication of brain-derived PrP^{Sc} using normal brain homogenate as a substrate (8). Here, we used a similar procedure to test whether structurally well-defined amyloid fibrils generated from moPrP23-144 can act as a seed to initiate conformational conversion of full-length PrP^{C} present in normal mouse brain homogenate (NMBH). Following each round of PMCA, the samples were treated with proteinase K and analyzed by gel electrophoresis and Western blotting. As shown in Fig. 1*A*, first-round PMCA reaction in the presence of moPrP23-144 fibril seed yielded relatively short PrP^{res} fragments of ~6–11 kDa and a small amount of longer PrP^{res} fragment(s). In the second round of PMCA (i.e., when the product of the first PMCA round was used as a seed), the longer fragments became much more prominent, displaying a ladder of four electrophoretic bands between ~17 kDa and 32 kDa. The latter bands have a different profile compared with those observed in a typical scrapie strain, ME7 (Fig. 1*A*, *Right*). In the latter case, there are three bands (corresponding to di-, mono-, and nonglycosylated PrP), and the positions of these bands suggest somewhat different sizes of PrP^{res} fragments from those in the product of the fibril-seeded PMCA reaction. Both types of PrP^{res} fragments observed in PMCA reaction (i.e., ~6–11 kDa and ~17–32 kDa) could be readily replicated in the third and subsequent rounds of PMCA. No PK-resistant product could be detected when PMCA experiments under identical conditions were performed without any seed (Fig. 1*A*) or in the presence of the moPrP23-144 monomer (Fig. S2). Importantly, because the 3F10 antibody used (epitope: PrP residues 135–150) does not recognize moPrP23-144 (Fig. S3), none of the PrP^{res} fragments seen in Fig. 1*A* could originate from the synthetic seed. Thus, the present data clearly demonstrate that amyloid fibrils prepared from the N-terminal fragment 23–144 of mouse PrP have the ability to induce (seed) the conversion of full-length mouse PrP^{C} to the PK-resistant form.

Next we tested whether PMCA conversion of PrP^{C} to PrP^{res} could also be triggered by amyloid fibrils generated from the full-length mouse PrP (moPrP23-230). moPrP23-230 fibrils used in this study, which are characterized by major PK-resistant fragments corresponding to residues 138/141–230 and 153–230 (Fig. S1), were totally ineffective as seeds in our PMCA experiments, as indicated by the lack of any PrP^{C}-derived PrP^{res} fragments (Fig. 1*B*).

moPrP23-144 Amyloid Fibrils Cause Transmissible Prion Disease in Mice. Building on intriguing data in vitro, next we tested the infectivity of moPrP23-144 amyloid fibrils in *tga20* mice, a frequently used model for studying transmissibility of prion diseases. These mice overexpress PrP^{C} and exhibit abbreviated incubation periods (61–88 d) for classical murine prion strains such as RML, 22L, or ME7 (26, 27), but they do not spontaneously develop any neurological disease or PrP brain plaques during lifetimes up to 900 d (28). Remarkably, all *tga20* mice inoculated with moPrP23-144 fibrils became clinically sick (Fig. 2*A*), with an average incubation time of 254 ± 12 d. Clinical signs included kyphosis, cerebellar ataxia, aberrant gait, weight loss, and hind-limb clasping. By contrast, none of PrP23-144 monomer- or PBS-inoculated mice showed any symptoms when monitored up to 600–700 d postinoculation.

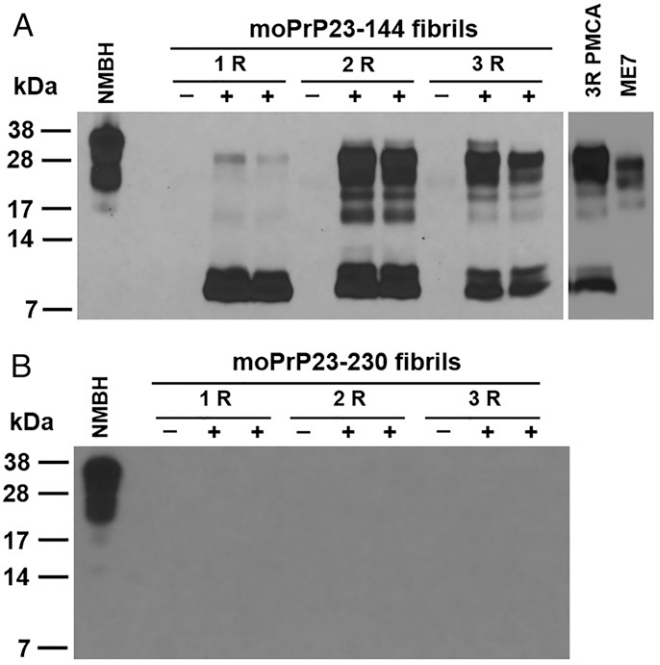

Fig. 1. Generation of PrP^{res} using moPrP23-144 fibrils as a seed in serial PMCA reaction. (*A*) NMBH was subjected to serial rounds (R) of PMCA in the presence (+) or absence (–) of moPrP23-144 fibril seed (first round) or previous-round PMCA product seed. As a reference, electrophoretic profile for ME7 scrapie strain is included in the *Right* panel. (*B*) NMBH was subjected to serial rounds (R) of PMCA in the presence (+) or absence (–) of moPrP23-230 fibrils seed (first round) or previous-round PMCA product seed. Western blots of PK-digested PMCA products are shown except in the first lane, in which the electrophoretic profile of undigested NMBH is shown. Numbers on the left represent molecular mass in kilodaltons. All blots were probed with 3F10 antibody (epitope: residues 135–150). The 3F10 antibody does not recognize moPrP23-144.

To test whether a disease caused by moPrP23-144 amyloid fibrils is transmissible, we inoculated healthy young *tga20* mice with brain homogenate derived from terminally sick fibril-inoculated *tga20* mice. All animals in this experiment developed a clinical disease. Although neurological signs were indistinguishable from those observed in *tga20* mice inoculated with original moPrP23-144 fibrils, the incubation time in the second-passage experiment decreased to 215 ± 19 d, suggesting a modest adaptation process (Fig. 2*A* and Fig. S4). We then performed a third-passage experiment, using brain homogenate from the second passage as the inoculum (Fig. 2*A* and Fig. S4). Again, all inoculated mice developed neurologic symptoms, with an average incubation time (208 ± 10 d) that was similar (no statistically significant difference) to that in the second-passage experiment.

Western blot (WB) analysis of brain homogenate from fibril-inoculated *tga20* mice revealed the presence of two types of PrP^{res} fragments: the longer fragments with molecular mass of ~17–32 kDa and the shorter ones migrating as ~6- to 11-kDa proteins (Fig. 2*B*). No PK-resistant material was detected in brain homogenate from *tga20* mice inoculated with moPrP23-144 monomer (Fig. 2*B*, lane 2). Comparison of longer PK-resistant fragments with those observed in a typical scrapie strain, ME7, reveals a different distribution of PrP^{res} isoforms (Fig. 2*B*, *Right*). Fibril-inoculated mice exhibited a predominant species corresponding to diglycosylated PrP, a much smaller quantity of

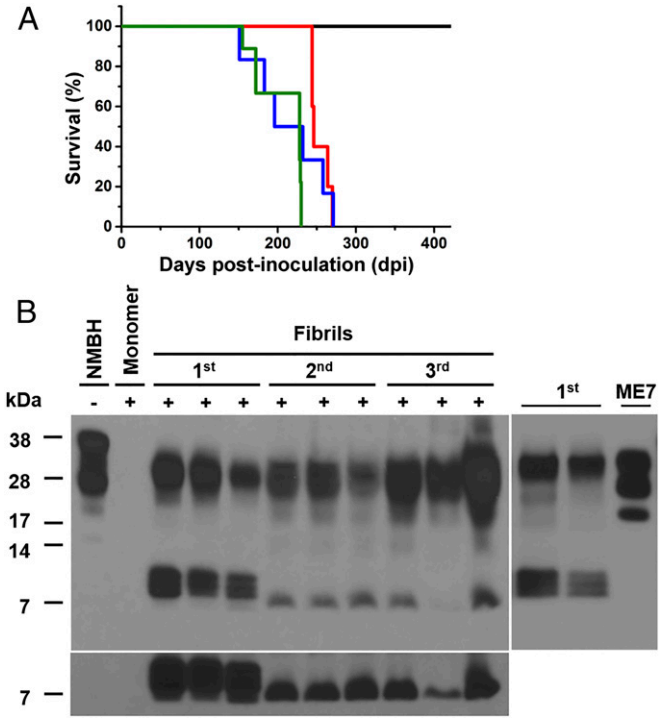

Fig. 2. moPrP23-144 fibrils induce transmissible prion disease in *tga20* mice. (*A*) Survival curves for moPrP23-144 fibril-inoculated *tga20* mice. In the first passage, mice were inoculated with moPrP23-144 fibrils in PBS. In subsequent passages, mice were inoculated with brain homogenates from previous passage mice. For control experiments, mice were inoculated with moPrP23-144 monomer in PBS (black, $n = 9$). The mean incubation periods were 254 ± 12 d in the first passage (red, $n = 5$), 215 ± 19 d in the second passage (blue, $n = 6$), and 208 ± 10 d in the third passage (green, $n = 8$). Data points on the *y* axis refer to survival of mice showing clinical signs including ataxic gait, kyphosis, and weight loss. (*B*) Detection of PrP^{res} in moPrP23-144 fibril-inoculated *tga20* mice and subsequent passage mice. Brains from terminally ill mice were treated with PK (+) and subjected to Western blot analysis. Data for three mice are shown for each passage experiment. The first lane shows data for PK-untreated (–) NMBH. Control data for PK-treated brain homogenate from moPrP23-144 monomer-inoculated *tga20* mice is shown in the second lane. (*Bottom*) Part of the blot after longer exposure. (*Right*) As a reference, the electrophoretic profile for the ME7 scrapie strain is included. Numbers on the left represent molecular mass in kilodaltons. Blots were probed with 3F10 antibody (which does not recognize moPrP23-144).

monoglycosylated isoform, and only trace amounts of nonglycosylated PrP^{res}. It should also be noted that, despite an overall similarity, the electrophoretic profile of longer PrP^{res} fragments in fibril-inoculated mice is not identical to that of PrP^{res} generated by fibril-seeded PMCA reaction (compare *Right* panels in Figs. 1*A* and 2*B* in relation to a common reference of ME7 scrapie strain).

The electrophoretic profiles of PrP^{res} in brain homogenates of *tga20* mice from the second- and third-passage experiments were generally similar to that observed for PrP^{res} from the first passage (Fig. 2*B*). However, as opposed to multiple low molecular bands (~6–11 kDa) seen in WB after the first passage, only single ~6- to 7-kDa band(s) were observed in brain homogenates from the second- and third-passage experiments.

Brains of fibril-inoculated *tga20* mice showed histopathology characteristic of prion diseases, with similar topography of spongiform degeneration at all three passages. The regions most strongly affected included the cerebral cortex, the hippocampus, and basal ganglia (Fig. 3 *A* and *B*). Furthermore, significant loss of granule cells was consistently observed in the cerebellum (Fig. 3*B*). Immunohistochemistry showed fine PrP-positive granules throughout the brain in both gray and white matter at all passages (Fig. 3*B* and Fig. S5). Furthermore, extensive PrP-positive plaques were observed at the border between the dorsal hippocampus and the hemispheric white matter as well as in periventricular regions, but only in the first-passage mice (Fig. 3*B* and Fig. S6). It should be noted that the PrP deposits were detected with the antibody SAF84 (epitope: PrP residues 160–170). Because this antibody does not recognize moPrP23-144 used as the initial inoculum, these deposits clearly originate from the endogenous PrP^{C}. Very similar patterns of spongiform degeneration in all three passages suggest that spongiosis correlates with the presence of PrP-positive granules, but not PrP plaques, as the latter are visible in the first-passage mice only. The identity of PrP fragments associated with these plaques is at present unknown.

Next, we tested the infectivity of moPrP23-144 fibrils in wild-type (FVB) mice. Also in this case, fibrils caused clinical disease with

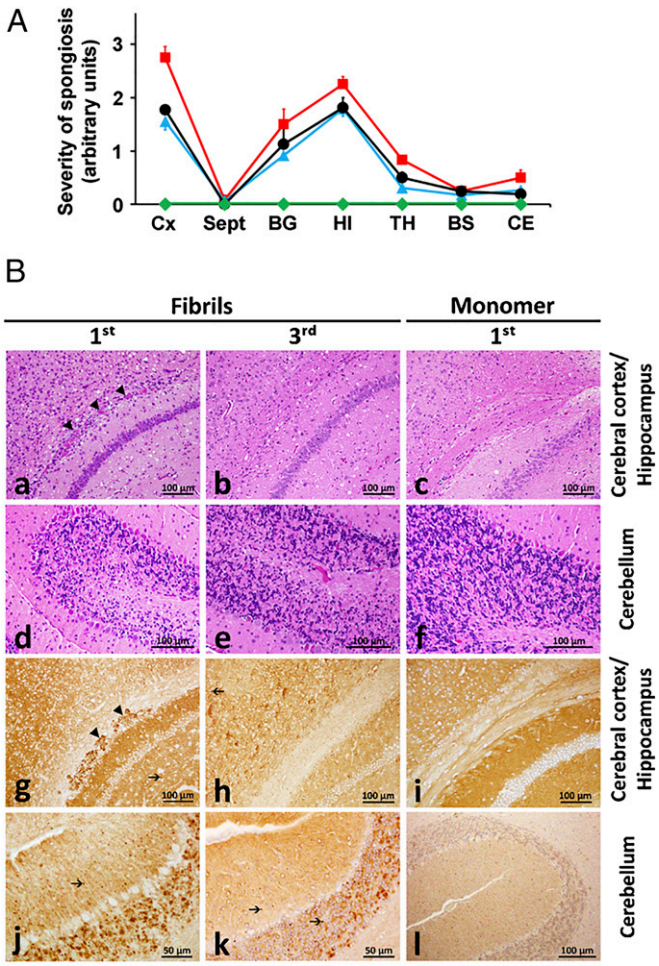

Fig. 3. Lesion profiles and histopathology of *tga20* mice inoculated with moPrP23-144 fibrils. (*A*) The profiles of spongiform degeneration in fibril-inoculated mice in the first (red), second (blue), and third (black) passage. No lesions were detected in monomer-inoculated mice (green). Symbols used for brain regions are the following: Cx, cerebral cortex; Sept, septal nuclei; BG, basal ganglia; HI, hippocampus; TH, thalamus; BS, brainstem; CE, cerebellum. Bars indicate SE. (*B*) Histological and immunochemical analysis of selected brain regions. Sections of cerebral cortex and cerebellum were analyzed by hematoxylin and eosin staining (*a*–*f*) and by PrP immunohistochemistry (*g*–*l*). Spongiform degeneration in cerebral cortex and loss of granule cells in the cerebellum were observed in fibril-inoculated mice at all passages, but not in monomer-inoculated mice. PrP plaques at the border between the alveus of the hippocampus and corpus callosum observed in the first-passage mice only are marked with arrowheads in *a* and *g*. Arrows mark selected PrP-positive granules (see also Fig. S5). PrP staining was performed using SAF84 antibody (which does not recognize moPrP23-144).

a 100% percent attack rate and incubation time of 534 ± 54 d (Fig. 4*A*). WB analysis revealed the presence of PK-resistant fragments that were similar to those described above for *tga20* mice (Fig. 4*B*). Large variability of incubation times among fibril-inoculated wild-type mice (308–670 d) showed no correlation with relative proportions of long and short PK-resistant fragments (Table S1). Histological examination of fibril-inoculated FVB mice showed focal spongiform degeneration affecting the hippocampus and, to a lesser degree, the brainstem (Fig. 4 *C* and *D*). The overall degree of spongiosis in these mice was substantially lower and had different distribution compared with that observed in *tga20* mice (Fig. 3*A*). There was no appreciable loss of granule cells in the cerebellum. PrP-positive plaques, often forming clusters, were present in the same brain regions as in fibril-inoculated *tga20* mice (Fig. 4*D*), even though the tinctorial characteristics of these plaques appeared distinct from those observed in *tga20* mice (Fig. S6). Immunohistochemistry showed no PrP granules. Low-severity focal spongiosis in moPrP23-144–inoculated wild-type mice is reminiscent of the neuropathology observed in some cases of GSS (19) and upon transmission of variably protease-sensitive prionopathy in mice (29).

Biochemical Characteristics of PrP^{res} in Fibril-Infected Mice. Upon deglycosylation using PNGase F, electrophoretic bands representing different glycoforms of large PrP^{res} fragments in brains of fibril-inoculated *tga20* or FVB mice were reduced to a single ∼17- to 18-kDa band (Fig. S7). This fragment appears to be slightly smaller than the deglycosylated PrP^{res} of ∼19 kDa observed in typical scrapie strains (30), the electrophoretic profile for one of which (139A) is included as a reference in Fig. S7. The molecular mass of smaller fragments remained unchanged upon treatment with PNGase F, indicating that these smaller fragments originate from the PrP region N-terminal to the glycosylation sites (residues 180 and 196). To further define the identity of these smaller PK-resistant fragments, WB were probed using a panel of monoclonal antibodies that recognize different linear epitopes of PrP (Fig. S8 and Table S2). This epitope mapping analysis indicates that the smallest (6–7 kDa) PK-resistant fragment (consistently seen in all three passages in *tga20* mice and in a single passage in FVB mice) has an N terminus between residues ∼80 and 89 and the C terminus between residues ∼150 and 159. The longer ∼10- to 11-kDa fragments (seen in brains after the first passage only) appear to have an N terminus that is similar to that of the 6- to 7-kDa fragment (within the resolution limit of the present epitope mapping), but extend C-terminally to at least residue 162–170.

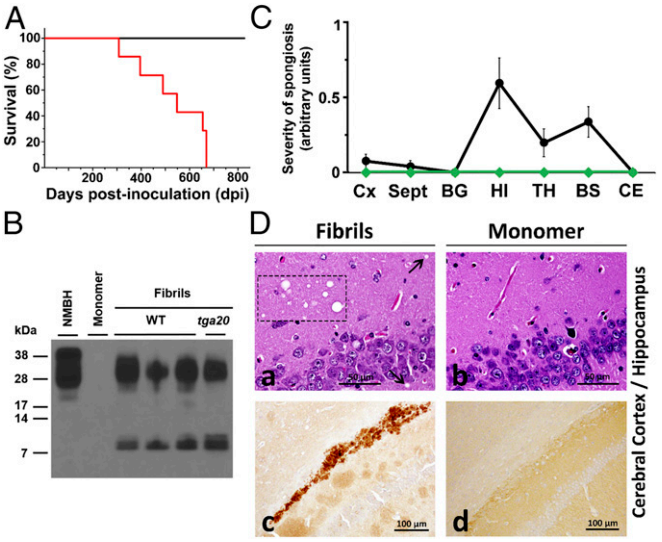

Fig. 4. moPrP23-144 fibrils induce prion disease in wild-type mice. (*A*) Survival curve for moPrP23-144 fibril-inoculated wild-type mice (red, $n = 7$). Black line represents control data for mice inoculated with moPrP23-144 monomer ($n = 8$). (*B*) Detection of PrP^{res} in moPrP23-144 fibril-inoculated wild-type mice. Brains from terminally ill mice were treated with PK and subjected to Western blot analysis. The first lane shows data for PK-untreated NMBH. Control data for PK-treated brain homogenate from moPrP23-144 monomer-inoculated mice is shown in the second lane. For comparison, the electrophoretic profile for PrP^{res} from fibril-inoculated *tga20* mice is shown in the last lane. Numbers on the left represent molecular mass in kilodaltons. The blot was probed with 3F10 antibody. (*C*) Lesion profiles of spongiform degeneration in fibril-inoculated wild-type mice (black). No lesions were detected in monomer-inoculated mice (green). Symbols used for brain regions are the following: Cx, cerebral cortex; Sept, septal nuclei; BG, basal ganglia; HI, hippocampus; TH, thalamus; BS, brainstem; CE, cerebellum. Bars indicate SE. (*D*) Histopathology of wild-type mice inoculated with moPrP23-144 fibrils. Sections of hippocampus were analyzed by hematoxylin and eosin staining (*a* and *b*) and by PrP immunochemistry (*c* and *d*). Clustered (dashed rectangle) and isolated (arrows) vacuoles were observed in fibril-inoculated mice (*a*), but not in monomer-inoculated mice (*b*). Clustered PrP plaques located between dorsal hippocampus and the hemispheric white matter were observed in fibril-inoculated mice (*c*), but not in monomer-inoculated mice (*d*). PrP staining was performed using SAF84 antibody.

Discussion

The principal finding of this study is that amyloid fibrils generated from the recombinant mouse prion protein N-terminal fragment 23–144 cause clinical prion disease, both in *tga20* mice that overexpress PrP and in wild-type mice. The incubation periods of the disease (∼210 and over 500 d in *tga20* and wild-type mice, respectively) are much longer compared with those observed for classical mouse-adapted scrapie strains such as RML, 22L, or ME7 (70–85 d and ∼140–200 d in *tga20* and wild-type mice, respectively) (26, 27). However, the apparent lack of any adaptation (shortening of the incubation time) between the second and third passage in *tga20* mice strongly suggests that these relatively long incubation periods are not due to low infectivity titer but, rather, represent an intrinsic property of this particular prion strain. Atypically long incubation periods have also been observed for some other prion strains such as mouse-adapted CWD or 87V (27).

An intriguing feature of prion disease caused by moPrP23-144 fibrils is the presence of two types of PrP^{res} fragments in mouse brains. The shorter 6- to 7-kDa fragments are reminiscent of human PrP^{res} observed in GSS subtypes (18–20) and amyloids found in GSS-like disease associated with the 145Stop mutation (22). The longer PrP^{res} fragment(s), on the other hand, are similar to those observed in classical mouse-adapted scrapie strains. The presence of both types of PrP^{res} fragments is highly unusual, clearly indicating the unique strain properties of prion disease described in this study. This rules out the possibility that the infectivity of the inoculum used in the first passage (i.e., moPrP23-144 fibrils) is due to a contamination with prions previously used in the laboratory. Altogether, data presented in this study clearly demonstrate that synthetic moPrP23-144 amyloid fibrils are infectious.

Previously, highly infectious prions that cause TSE disease in wild-type mice have been generated de novo using PMCA procedures from purified brain-derived PrP^{C} or bacterially expressed recombinant PrP, but only in the presence of RNA molecules and copurified lipids (4) or RNA and the synthetic acidic phospholipid, phosphatidylglycerol (5). It was also shown that infectious prions can be propagated in a PrP^{Sc}-seeded PMCA reaction using recombinant PrP and a naturally occurring phospholipid, phosphatidylethanolamine, as a solitary cofactor (6). These studies suggest that cofactors such as RNA and/or certain lipids are integral and essential components of mammalian prions, playing a crucial role in the formation and maintenance of specific PrP^{Sc} conformations that define prion infectivity and strain properties (6).

An alternative approach to the creation of synthetic prions involves incubation of bacterially expressed recombinant full-length PrP or its C-terminal fragment 89–230 (that encompasses the entire folded domain of PrP) in the presence of chemical denaturants that promote partial unfolding of the protein and its conversion to amyloid fibrils. Depending on the preparation

method (buffer pH, concentration of chaotropes, annealing treatment), such fibrils appear to have distinct physicochemical properties, showing differences in conformational stability, packing arrangement within the core region, and the size of PK-resistant fragments (11–17, 31). Unlike moPrP23-230 fibrils used as a control in our present study, one preparation of full-length PrP fibrils (characterized by longer PK-resistant species, ranging from an apparently intact protein to 17- to 19-kDa fragments) was recently reported to seed PrP^C conversion in the PMCA reaction (17). Detailed biophysical studies are needed to determine the structural basis of distinct patterns of PK-resistant species in different preparations of moPrP23-230 fibrils as well as the relationship between specific structural features and seeding capacity in PMCA reactions.

Various preparations of amyloid fibrils from full-length PrP or the 89–230 fragment were reported to cause prion disease in different lines of transgenic mice that either overexpress wild-type or mutated forms of PrP (10–12) or express PrP lacking the GPI anchor (16). A disease was also reported upon multiple serial passages of some of these preparations in hamsters (13–15). However, in no case were clinical symptoms found upon primary passage of synthetic PrP amyloid fibrils in wild-type animals, including direct inoculation with fibrils reported to seed PrP^C conversion in the PMCA reaction (17).

Amyloid fibrils used in the present study were prepared from the N-terminal fragment of PrP. In a monomeric form, this fragment is largely unstructured, forming amyloid fibrils under physiological buffer conditions in the absence of any denaturants or other cofactors (23). Remarkably, unlike fibrils generated from the full-length rPrP or the C-terminal fragment 89–230, moPrP23-144 fibrils cause clinical prion disease upon first passage not only in transgenic mice overexpressing PrP^C, but also in wild-type mice. The finding that moPrP23-144 amyloid fibrils generated in the absence of any cofactors cause TSE disease in wild-type animals provides strong (arguably the strongest to date) support for the protein-only hypothesis in its pure form. These data also argue against the notion that specific non-proteinaceous cofactors are obligatory structural components of all infectious prions, even though such cofactors may play an important regulatory role, acting as strain-specific modulators of prion replication and their biological properties.

One of major unresolved issues in TSE research relates to the structural basis of prion protein conversion to the infectious form, and there has been a major dispute as to whether the architecture of infectious prions is based on a β-helix motif or a parallel in-register β-structure (32, 33). A β-solenoid–type architecture for at least one mammalian prion strain has been identified in a recent electron cryomicroscopic study with brain-derived GPI-anchorless PrP^{Sc} fibrils (34). Even though the latter study does not provide an atomic resolution picture, it revealed a four-rung β-solenoid structure as a basic building block of these fibrils. Whether a similar motif underlies the structure of more typical murine prion strains (that contain the GPI anchor) remains to be determined.

The present finding regarding infectivity of moPrP23-144 amyloid fibrils sheds light on the ongoing debate regarding the structure of mammalian prions, especially because—unlike brain-derived prions or PMCA-generated synthetic prions—these fibrils are amenable to high-resolution structural characterization using solid-state NMR spectroscopy. A series of such studies revealed that the rigid β-sheet core of these fibrils consists of three β-strands within the region between residues 112 and 139 and that this β-sheet core displays a parallel in-register organization (35–37). It is intriguing that fibrils with such a short core region have the capacity to seed the conversion of full-length PrP to a structure characterized by much longer PK-resistant fragment(s) resembling those observed in classical scrapie strains. The mechanism of this process likely involves binding of the ∼112–139 segment in the PrP^C monomer to the end of fibrillar seed, followed by templated conversion of this segment to the β-structure of the amyloid core of the seed. Remarkably,

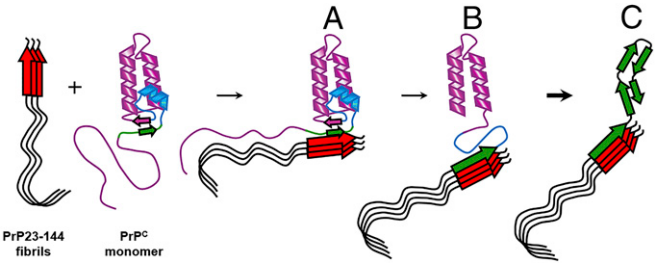

Fig. 5. Hypothetical mechanism of full-length prion protein conversion to the infectious form upon seeding with moPrP23-144 fibrils. (*A*) The ∼112–139 segment of the PrP^C monomer binds to the fibril β-sheet core (residues ∼112–139) that displays a parallel in-register organization. (*B*) Fibril-templated conversion of the ∼112–139 segment of the monomer to β-structure of the seed. (*C*) Extension of the β-sheet structure of the PrP^C substrate to the C-terminal region. The proposed model is schematic; it does not imply any specific structural organization of individual β-strands in the parallel in-register architecture of the fibrils.

initial formation of this relatively short β-core appears to be sufficient to trigger a reaction in which β-sheet structure extends to more terminal regions of PrP^{res}. This proposed mechanism for moPrP23-144 fibril-seeded conversion of full-length PrP^C is illustrated in Fig. 5.

The hypothetical mechanism discussed above assumes structural fidelity of the initial conversion step (i.e., the ∼112–139 segment of the PrP^C monomer undergoes templated conversion to the structure of the seed). Given that PrP23-144 amyloid displays a parallel in-register β-sheet arrangement, geometrical considerations dictate that, in this scenario, the entire β-sheet core of PrP^{res} formed upon seeding with moPrP23-144 fibrils should also have a parallel β-sheet architecture. An alternative possibility, however, is that moPrP23-144 fibrils merely induce the conversion of full-length PrP^C in a nontemplating fashion, possibly to a different self-propagating structure. Although the latter possibility seems less likely, it cannot be ruled in the absence of structural data for brain PrP^{Sc} generated upon infection with moPrP23-144 fibrils. The picture is further complicated by the presence of two distinct types of PK-resistant fragments in brains of moPrP23-144 fibril-inoculated mice, as these fragments may suggest two distinct conformations of PrP^{Sc}. In any case, the present findings, together with the recent structural data for GPI-anchorless prions (34), raise an intriguing possibility that entirely different structural motifs may be present in distinct prion strains.

Apart from providing direct evidence that infectious prions can be generated in vitro from a relatively small recombinant fragment of PrP in the absence of any cofactors and impacting the ongoing debate regarding structural determinants of infectivity, the present data strongly support recent assertions that GSS subtypes may have much higher potential for transmissibility than is generally appreciated (38, 39). In this context, it should be noted that an attempt to transmit human prion disease with the 145Stop mutation to mice (expressing murine PrP^C) has not been successful (40). However, this may be due simply to the lack of amino acid sequence identity between prion proteins in the inoculum and the host. Indeed, our preliminary data indicate that identity of certain residues is critical for the ability of PrP23-144 fibrils to seed the conversion of PrP^C in vitro by PMCA.

Materials and Methods

Recombinant Prion Proteins and Amyloid Fibril Formation. Recombinant mouse full-length prion protein (moPrP23-230) and its N-terminal fragment moPrP23-144 were expressed and purified as described previously (23, 41). Amyloid fibrils from moPrP23-144 were prepared by the procedure described by Vanik et al. (24) and those from moPrP23-230 as described previously (42). Fibril morphology was monitored using atomic force microscopy as described previously (25). Before inoculations, fibrils were resuspended in PBS and fragmented by two cycles of 15-s sonication on ice.

PMCA. NMBH from wild-type (FVB) mice was prepared as described before (9). Serial PMCA was performed using a general procedure described previously (8). Briefly, for the first-round reaction, 10-μL aliquots of moPrP23-144 or moPrP23-230 fibrils in PBS (final concentration 0.5 μM) were added to 90 μL of 10% NMBH and placed in 0.2-mL PCR tubes equipped with three 2.38-mm-diameter polytetrafluoroethylene beads. Tubes were positioned in a rack placed on the plate holder of a sonicator (Misonix Q700) thermostated at 37 °C and programmed to perform 48 cycles, each consisting of a 40-s pulse of sonication (30% sonicator potency) followed by 30 min of incubation. For subsequent rounds, PMCA products from the previous round were diluted 10-fold into 10% (wt/vol) NMBH, and the sonication/incubation cycles were repeated as described above. All equipment was cleaned between successive PMCA experiments by immersing in 100% bleach for 5 min with intermittent sonication.

Infectivity Bioassays. Transgenic mice *tga20* (43) were provided by Charles Weissmann, Scripps Research Institute, Jupiter, FL, and wild-type (FVB) mice were purchased from Charles River Laboratory. For first-passage bioassays, 6-wk-old mice were inoculated intracerebrally with moPrP23-144 fibrils in PBS (30 μL; 100 μg/mL). For subsequent passages, 30 μL of 1% (wt/vol) brain homogenate from terminally ill mice from the previous passage was used as the inoculum. Mice were monitored three times weekly, and diagnosis of prion disease was performed using standard criteria (44). Mice were euthanized upon confirmation of clinical symptoms or at the age of 650–800 d. All procedures involving animals were approved by the Institutional Animal Care and Use Committee of Case Western Reserve University.

Protease Digestion and Immunoblotting. To detect PrP^{res} in PMCA reactions, samples were treated with proteinase K (50 μg/mL) at 37 °C for 1 h. Immediately after treatment, lithium dodecyl sulfate denaturing buffer (Thermo Fisher Scientific) or Tricine sample buffer (Bio-Rad) was added, followed by heating at 100 °C for 10 min. To detect PrP^{res} in brain, 10% homogenates in PBS were prepared and treated with PK (25 μg/mL) as described above. Samples were analyzed by gel electrophoresis on 4–12% NuPAGE (Thermo Scientific) or 10–20% Criterion Tris–Tricine gel (Bio-Rad) and transferred onto nitrocellulose membrane. Blots were probed with anti-PrP monoclonal 3F10 antibody (1:10,000) (45), 1C5 (1:1,000) (45), SAF32 (1:2,000) (Cayman Chemical), SAF70 (1:2,000) (Cayman Chemical), SAF84 (1:1,000) (Cayman Chemical), or 12B2 (1:1,000) (Central Veterinary Institute of Wageningen UR) overnight at 4 °C. The blots were developed as described previously (9).

Neuropathology. Brains were fixed in 10% buffered formalin and embedded in paraffin. Staining with hematoxylin and eosin was performed on 5- to 8-μm-thick sections. PrP^{res} was detected using SAF84 monoclonal antibody (1:350 and 1:700). Semiquantitative evaluation of spongiosis in different regions of gray matter was performed by comparing hematoxylin and eosin-stained sections as described previously (9). Severity of SD and neuronal loss was scored on a 0–4 scale (9).

ACKNOWLEDGMENTS. We thank Xiangzhu Xiao for performing mass spectrometric analysis of PrP fibrils, Diane Kofskey for preparing samples for histologic and immunochemical analysis, and W. Michael Babinchak for critically reading the manuscript. This study was supported in part by NIH Grants P01 AI106705 and R01 NS083687 and the Britton Fund.

1. Prusiner SB (1998) Prions. *Proc Natl Acad Sci USA* 95(23):13363–13383.
2. Aguzzi A, Sigurdson C, Heikenwaelder M (2008) Molecular mechanisms of prion pathogenesis. *Annu Rev Pathol* 3:11–40.
3. Cobb NJ, Surewicz WK (2009) Prion diseases and their biochemical mechanisms. *Biochemistry* 48(12):2574–2585.
4. Deleault NR, Harris BT, Rees JR, Supattapone S (2007) Formation of native prions from minimal components in vitro. *Proc Natl Acad Sci USA* 104(23):9741–9746.
5. Wang F, Wang X, Yuan CG, Ma J (2010) Generating a prion with bacterially expressed recombinant prion protein. *Science* 327(5969):1132–1135.
6. Deleault NR, et al. (2012) Isolation of phosphatidylethanolamine as a solitary cofactor for prion formation in the absence of nucleic acids. *Proc Natl Acad Sci USA* 109(22): 8546–8551.
7. Büeler H, et al. (1993) Mice devoid of PrP are resistant to scrapie. *Cell* 73(7):1339–1347.
8. Castilla J, Saá P, Hetz C, Soto C (2005) In vitro generation of infectious scrapie prions. *Cell* 121(2):195–206.
9. Kim JI, et al. (2010) Mammalian prions generated from bacterially expressed prion protein in the absence of any mammalian cofactors. *J Biol Chem* 285(19): 14083–14087.
10. Legname G, et al. (2004) Synthetic mammalian prions. *Science* 305(5684):673–676.
11. Legname G, et al. (2006) Continuum of prion protein structures enciphers a multitude of prion isolate-specified phenotypes. *Proc Natl Acad Sci USA* 103(50):19105–19110.
12. Colby DW, et al. (2009) Design and construction of diverse mammalian prion strains. *Proc Natl Acad Sci USA* 106(48):20417–20422.
13. Makarava N, et al. (2010) Recombinant prion protein induces a new transmissible prion disease in wild-type animals. *Acta Neuropathol* 119(2):177–187.
14. Makarava N, et al. (2011) Genesis of mammalian prions: from non-infectious amyloid fibrils to a transmissible prion disease. *PLoS Pathog* 7(12):e1002419.
15. Makarava N, et al. (2012) A new mechanism for transmissible prion diseases. *J Neurosci* 32(21):7345–7355.
16. Raymond GJ, et al. (2012) Isolation of novel synthetic prion strains by amplification in transgenic mice coexpressing wild-type and anchorless prion proteins. *J Virol* 86(21): 11763–11778.
17. Moda F, et al. (2015) Synthetic prions with novel strain-specified properties. *PLoS Pathog* 11(12):e1005354.
18. Parchi P, et al. (1998) Different patterns of truncated prion protein fragments correlate with distinct phenotypes in P102L Gerstmann-Sträussler-Scheinker disease. *Proc Natl Acad Sci USA* 95(14):8322–8327.
19. Piccardo P, et al. (1998) Phenotypic variability of Gerstmann-Sträussler-Scheinker disease is associated with prion protein heterogeneity. *J Neuropathol Exp Neurol* 57(10):979–988.
20. Tagliavini F, et al. (2001) A 7-kDa prion protein (PrP) fragment, an integral component of the PrP region required for infectivity, is the major amyloid protein in Gerstmann-Sträussler-Scheinker disease A117V. *J Biol Chem* 276(8):6009–6015.
21. Kitamoto T, Iizuka R, Tateishi J (1993) An amber mutation of prion protein in Gerstmann-Sträussler syndrome with mutant PrP plaques. *Biochem Biophys Res Commun* 192(2):525–531.
22. Ghetti B, et al. (1996) Vascular variant of prion protein cerebral amyloidosis with tau-positive neurofibrillary tangles: The phenotype of the stop codon 145 mutation in PRNP. *Proc Natl Acad Sci USA* 93(2):744–748.
23. Kundu B, et al. (2003) Nucleation-dependent conformational conversion of the Y145Stop variant of human prion protein: Structural clues for prion propagation. *Proc Natl Acad Sci USA* 100(21):12069–12074.
24. Vanik DL, Surewicz KA, Surewicz WK (2004) Molecular basis of barriers for interspecies transmissibility of mammalian prions. *Mol Cell* 14(1):139–145.
25. Jones EM, Surewicz WK (2005) Fibril conformation as the basis of species- and strain-dependent seeding specificity of mammalian prion amyloids. *Cell* 121(1):63–72.
26. Thackray AM, Klein MA, Aguzzi A, Bujdoso R (2002) Chronic subclinical prion disease induced by low-dose inoculum. *J Virol* 76(5):2510–2517.
27. Bett C, et al. (2012) Biochemical properties of highly neuroinvasive prion strains. *PLoS Pathog* 8(2):e1002522.
28. Sigurdson CJ, et al. (2009) De novo generation of a transmissible spongiform encephalopathy by mouse transgenesis. *Proc Natl Acad Sci USA* 106(1):304–309.
29. Notari S, et al. (2014) Transmission characteristics of variably protease-sensitive prionopathy. *Emerg Infect Dis* 20(12):2006–2014.
30. Taraboulos A, et al. (1990) Acquisition of protease resistance by prion proteins in scrapie-infected cells does not require asparagine-linked glycosylation. *Proc Natl Acad Sci USA* 87(21):8262–8266.
31. Cobb NJ, Apostol MI, Chen S, Smirnovas V, Surewicz WK (2014) Conformational stability of mammalian prion protein amyloid fibrils is dictated by a packing polymorphism within the core region. *J Biol Chem* 289(5):2643–2650.
32. Surewicz WK, Apostol MI (2011) Prion protein and its conformational conversion: a structural perspective. *Top Curr Chem* 305:135–167.
33. Diaz-Espinoza R, Soto C (2012) High-resolution structure of infectious prion protein: The final frontier. *Nat Struct Mol Biol* 19(4):370–377.
34. Vázquez-Fernández E, et al. (2016) The structural architecture of an infectious mammalian prion using electron cryomicroscopy. *PLoS Pathog* 12(9):e1005835.
35. Helmus JJ, Surewicz K, Nadaud PS, Surewicz WK, Jaroniec CP (2008) Molecular conformation and dynamics of the Y145Stop variant of human prion protein in amyloid fibrils. *Proc Natl Acad Sci USA* 105(17):6284–6289.
36. Helmus JJ, Surewicz K, Surewicz WK, Jaroniec CP (2010) Conformational flexibility of Y145Stop human prion protein amyloid fibrils probed by solid-state nuclear magnetic resonance spectroscopy. *J Am Chem Soc* 132(7):2393–2403.
37. Helmus JJ, Surewicz K, Apostol MI, Surewicz WK, Jaroniec CP (2011) Intermolecular alignment in Y145Stop human prion protein amyloid fibrils probed by solid-state NMR spectroscopy. *J Am Chem Soc* 133(35):13934–13937.
38. Asante EA, et al. (2013) Inherited prion disease A117V is not simply a proteinopathy but produces prions transmissible to transgenic mice expressing homologous prion protein. *PLoS Pathog* 9(9):e1003643.
39. Pirisinu L, et al. (2016) Gerstmann-Sträussler-Scheinker disease subtypes efficiently transmit in bank voles as genuine prion diseases. *Sci Rep* 6:20443.
40. Tateishi J, Kitamoto T (1995) Inherited prion diseases and transmission to rodents. *Brain Pathol* 5(1):53–59.
41. Morillas M, Swietnicki W, Gambetti P, Surewicz WK (1999) Membrane environment alters the conformational structure of the recombinant human prion protein. *J Biol Chem* 274(52):36859–36865.
42. Apetri AC, Vanik DL, Surewicz WK (2005) Polymorphism at residue 129 modulates the conformational conversion of the D178N variant of human prion protein 90-231. *Biochemistry* 44(48):15880–15888.
43. Fischer M, et al. (1996) Prion protein (PrP) with amino-proximal deletions restoring susceptibility of PrP knockout mice to scrapie. *EMBO J* 15(6):1255–1264.
44. Carlson GA, et al. (1988) Genetics and polymorphism of the mouse prion gene complex: Control of scrapie incubation time. *Mol Cell Biol* 8(12):5528–5540.
45. Choi JK, et al. (2006) Generation of monoclonal antibody recognized by the GXXXG motif (glycine zipper) of prion protein. *Hybridoma (Larchmt)* 25(5):271–277.